Građevinski materijali i konstrukcije
Building Materials and Structures

journal homepage: www.dimk.rs

https://doi.org/10.5937/GRMK2300004N

**Original scientific paper**

# Numerical modelling of concrete-filled steel tubular short columns under axial compression

Jelena Nikolić[*1)], Svetlana M. Kostić[1)], Saša Stošić[1)]

[1)] *University of Belgrade, Faculty of Civil Engineering, Department of Engineering Mechanics and Theory of Structure, Bulevar kralja Aleksandra 73, 11000 Belgrade, Serbia*

*Article history*

*Received:* 25 January 2023
*Received in revised form:* 07 April 2023
*Accepted:* 04 May 2023
*Available online*: 09 June 2023

*Keywords*

composite columns,
nonlinear analysis,
3D FEM model,
concrete material model,
Eurocode 4

*ABSTRACT*

The paper presents three-dimensional numerical models of short concrete-filled steel tubular circular columns that can successfully describe the column behaviour under axial compression. Several of the most commonly used material models for the steel part and a concrete portion of the column are evaluated in the models. In addition, the paper presents a new proposal for the extension of the Eurocode 2 stress-strain relation to make it suitable for describing the complex behaviour of concrete inside the steel tube. This model overcomes the current limitations of the Eurocode 2 design guide, referring to the limitation for the concrete curve in compression to 3.5‰ strain. The ultimate axial column strength obtained by the proposed model is compared to the ultimate column capacity calculated by a simplified method provided in Eurocode 4. All presented numerical models are validated on a set of experiments from the literature and demonstrate good agreement. The comments about the accuracy of each model are provided, along with the identified limitations.

## 1 Introduction

A concrete-filled steel tubular column (CFST) consists of an outer steel tube filled with concrete. The composite action between the two parts, the concrete core and steel tube, ensures that the concrete core stiffens the steel tube and postpones its local buckling. In turn, the outer steel tube acts as longitudinal and transverse reinforcement, permanent formwork, and confinement for the concrete core. CFST columns demonstrate excellent structural behaviour, such as high strength, stiffness, ductility, and good seismic behaviour [1], [2].

Due to their overall good performance, CFST columns have been widely used in different types of construction and are the subject of numerous ongoing research projects [1]. Various shapes and types of CFST columns have been constructed in the past [3]–[6]. The axial behaviour of these columns has been investigated experimentally and numerically. To date, several databases with experimental results exist, counting more than one thousand axially loaded specimens [7].

In general, there are three approaches to the numerical modelling of CFST columns. The first uses the simplified concentrated plasticity nonlinear beam/column elements [2], [7]. These elements are computationally very efficient but have some limitations since they require the expressions of the yield surface, which depend on the column cross-section. The second approach deals with the distributed plasticity fibre beam-column elements [8]–[10]. Although slightly less computationally efficient than elements from the first group, these numerical models are much more versatile and can account for numerous nonlinear effects, such as the nonlinear material behaviour of constituent parts, residual stresses, and nonlinear geometry. However, they can capture only indirectly the local buckling of the steel tube, the interaction of the steel tube with the concrete part, and the variable confinement effects of the concrete core. For these reasons, there is a need to develop reliable, sophisticated, 3D finite element models that can fully describe the complex nonlinear behaviour of the composite columns. These models can also predict other important information, such as failure modes and deformation patterns, or capture phenomena such as local buckling of the steel tube and confinement of the concrete part of the section [11]. This third approach is followed in this paper.

There are several 3D numerical models developed in the past [12]–[14] using the commercial program ABAQUS. The crucial differences among these models are the assumed material model behaviour, initial imperfections and residual stresses, modelling the steel tube–concrete core interface, and the boundary conditions. Most of these models proposed their own concrete material models [13], [15]–[17] or steel material models [10], [13], [15], [16]. However, there is a lack of numerical models that deploy the material models proposed by the Eurocode design guide. For that reason, the study presented in this paper provides a relatively simple 3D

[*] Corresponding author:
*E-mail address* jnikolic@grf.bg.ac.rs

numerical model developed in the commercial program ABAQUS that follows the general analysis method of Eurocode 4 (EC4) for the nonlinear analysis of axially loaded CFST columns. The proposal for the extension of the concrete material model suggested by Eurocode 2 (EC2) is developed to make it suitable for describing the complex behaviour of concrete inside the steel tube. The developed concrete material model is carefully evaluated and compared with other commonly employed concrete material models. Finally, the ultimate strength results are compared to the axial capacity of the short columns calculated by EC4 [18], [19].

## 2 Numerical modelling of short cfst columns

The study presented here is focused on the efficient numerical modelling of short CFST columns. These columns are expected to develop a cross-section's full plastic strength capacity without failing due to buckling. According to the Japanese standard AIJ [20], CFST columns are classified as short columns when the length-to-outer column diameter ratio is less than or equal to four ($L/D \leq 4$) and this boundary is commonly used among researchers for the classification [9].

The numerical model of the CFST columns needs to predict structural members' behaviour effectively and provide complex information regarding their structural response. On the other side, the model needs to be relatively simple because of its computational efficiency. This paper presents one such model for the CFST short columns under axial loading. The model considers the geometry, the test setup simulation, boundary conditions, and applied loading in a simplified way. It is validated based on selected test results from the literature and previously developed models by other authors. The analysis is performed as the displacement controlled in all these simulations and includes material and geometrical nonlinearities. A detailed description of the developed numerical model follows.

### 2.1 3D model description

Finite element analysis (FEA) was conducted using ABAQUS [21] version 6.9, which offers significant capabilities for the 3D nonlinear analysis of CFST columns. ABAQUS Standard solver was chosen due to the quasi-static nature of the loading and its ability to analyse such conditions accurately. The possible disadvantage of 3D modelling is that many elements in the model may require a long calculation time. For the sake of reasonable time for both developing the 3D model and the analysis, the intention here was to create a simple but reliable model that would provide highly accurate results.

The outer steel tube and the concrete core are modelled using the 3D8-node brick elements (C3D8R) with reduced integration (i.e., one integration point), Figure 1. The element has three translation degrees of freedom at each element node. The single-point reduced-integration scheme is based on the “uniform strain formulation”, meaning that the strains are obtained as the average strain over the element volume. The advantage of the reduced integration elements comes from the fact that strains and stresses are calculated at locations that provide optimal accuracy. A second advantage is that the reduced number of integration points decreases calculation time and storage requirements [21]. For the steel tube, shell elements might be used as well, since they are generally well-suited for analysing structures with thin to moderately thick walls. In the presented analysis, using the shell elements for modeling steel tube would not have an effect on the results, as shown in Figure 2a below for test CC-0 with Model 4.

The boundary conditions at column ends are considered by applying the constraints option available in ABAQUS. It connects all surface nodes to only one reference point (RP) defined in the centre of the column's top and bottom surfaces, as shown in Figure 1. Tests used to validate the FE models had steel plates for load application at both ends of the specimens. Some tests had these plates welded at both ends of specimens [11], [22], while others used plates in a

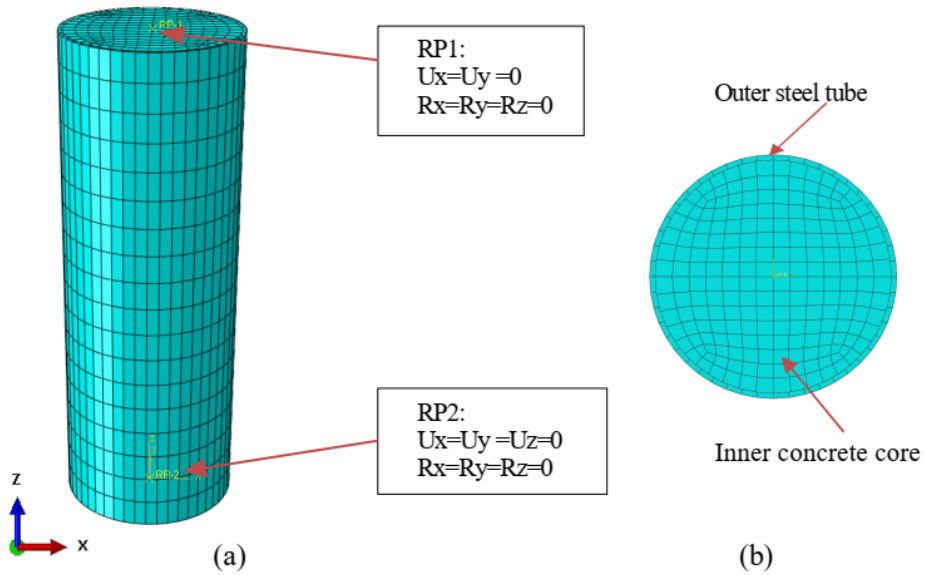


*Figure 1. (a) 3D model of CFST column with RP1 and RP2 with BC; (b) Cross-section and meshing*

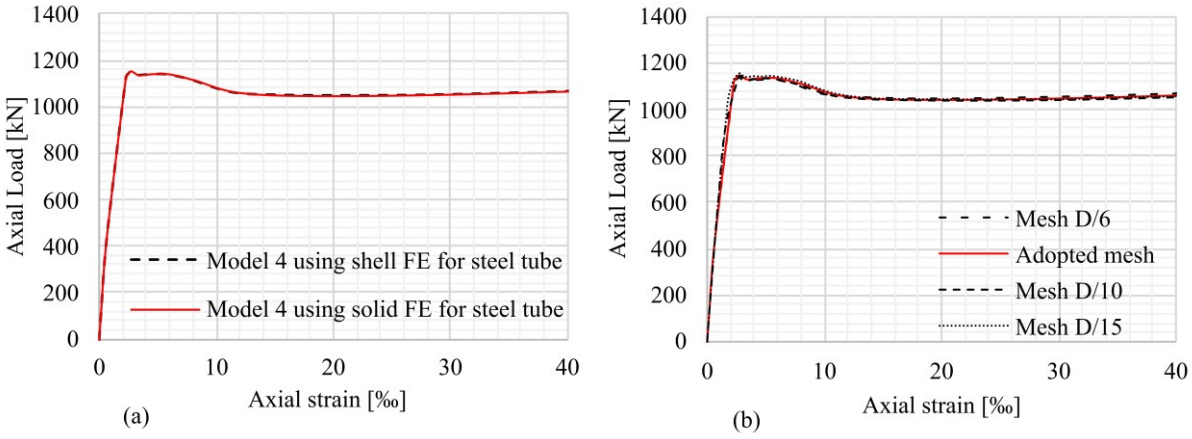


*Figure 2.(a) Mesh type sensitivity analysis on specimen CC-0 using Model 4; (b) Mesh size sensitivity analysis on specimen CC-0 using Model 4*

testing machine only to ensure load application to the whole cross-sections [23],[24]. Test boundary conditions are modelled numerically using the constraint option on specimen end surfaces. This is considered adequate since the steel plates were very stiff. The end surface behaves rigidly with a master node (RP). Boundary conditions (BC) are set to RP1 and RP2: all displacements are restrained except displacement in the loading direction at RP1. A displacement-controlled axial loading scheme is applied to the RP1 only.

The starting point for the selection of the FE mesh size were the conclusions from the mesh convergence studies presented in reference [13]. Accordingly, the optimal element size across the cross-section was determined to be $D/15$, where $D$ represents the outer diameter of a circular column. The element size in the longitudinal direction was 2.5 times larger than that in the cross-section. However, a mesh sensitivity study was conducted to confirm the convergence of results as well as the total computational time required for the analysis. Figure 2b shows the FEM mesh size sensitivity analysis for Model 4 for specimen CC-0 using the adopted mesh size and three other meshes, namely $D/6$, $D/10$, and $D/15$. As demonstrated, the results confirm convergence, particularly considering that the model with $D/15$ took almost ten times longer to run.

Interaction between the steel tube and the concrete core is simulated using the surface-to-surface contact option. The inner steel tube surface is chosen as the master surface, while the concrete surface is defined as the slave surface. When two surfaces are in contact, they transmit shear and normal forces across their interface. The normal (radial) contact behaviour is defined using the "hard" contact option. This relationship minimises the penetration of the slave surface into the master surface in compression and allows separation after contact. The tangential behaviour between surfaces is defined using the friction formulation with “penalty”. It uses the classical isotropic Coulomb friction model, where the critical shear stress is obtained as a contact pressure multiplied by a coefficient of friction. Some studies have investigated this particular effect [25], and the literature reports a coefficient range of 0.5 to 0.6 for carbon steel tubes. Our own investigation revealed that values between 0.4 and 0.7 had little impact on axial resistance. Therefore, we have adopted a friction coefficient of 0.6 in our models, as suggested in [16].

The initial local or global imperfections were not considered in the model as their influence was negligible for the stub columns that are the subject of this paper. Namely, specimens with $L/D \leq 3$ do not demonstrate lateral deflections during failure tests, and the concrete infill reduces some possible local imperfections of the steel tube [11]. However, the behaviour of columns with a higher $L/D$ ratio may be affected to a certain degree by global imperfections.

## 2.2 Material modelling

In this study, four different combinations of steel and concrete material models are assigned to the steel tube and the concrete core, as summarised in Table 1, and these models are evaluated. Therefore, all four 3D models, denoted as Models 1 to 4, have the same geometry, boundary conditions, and FE mesh but different assigned material models for steel tube and concrete core. Models 1, 2, and 3 follow the commonly applied material models as recommended by [13], [16], and [26], respectively. Model 4 is created using the material curves provided in Eurocode 3 (EC3) [27] for steel tubes and the proposed extended material model for concrete in Eurocode 2 (EC2) [28]. These modifications are explained in detail later in the paper.

*Table 1. Numerical models with details of material modelling*

| Model | Structural steel | Concrete |
|---|---|---|
| Model 1 | Tao et al. [13] | Tao et al. [13] |
| Model 2 | Han et al. [16] | Han et al. [16] |
| Model 3 | EC3 [27] | Ellobody [26] |
| Model 4 | EC3 [27] | proposed extended EC2 |

### 2.2.1 Material modelling of concrete core in ABAQUS

Concrete under compression initially exhibits an elastic response. As the stress increases, non-recoverable (inelastic) strains occur, and the material's stiffness decreases. After ultimate stress is reached, the material softens until it can no longer carry any stress. In multiaxial stress states, these observations can be generalised through

surfaces of failure and ultimate strength surfaces in stress space. These surfaces are fitted to the experimental data.

Under low confining pressures, concrete behaves in a brittle manner, so the main failure mechanisms are cracking in tension and crushing in compression. The brittle behaviour of concrete disappears when the confining pressure is sufficiently large to prevent crack propagation. Under these circumstances, failure is driven by the consolidation and collapse of the concrete´s microporous microstructure, leading to a macroscopic response resembling a ductile material with work hardening.

In ABAQUS, the concrete damage plasticity (CDP) model for quasi-brittle materials is the constitutive model commonly adopted for concrete. This CDP model is a plasticity-based continuum model. The elastic response is assumed to be linear and isotropic, defined by the modulus of elasticity and Poisson‘s ratio. The plastic region requires the definition of stress-strain curves for both compression and tension behaviour. Input parameters are stress values and the corresponding inelastic strain. The following strain rate decomposition is assumed for the model:

$$\dot{\varepsilon} = \dot{\varepsilon}^{el} + \dot{\varepsilon}^{pl} \tag{1}$$

where $\dot{\varepsilon}$ is the total strain rate, $\dot{\varepsilon}^{el}$ is the elastic part of the strain rate while $\dot{\varepsilon}^{pl}$ is the plastic part of the total strain [21].

The CDP model also requires the input of five plasticity parameters: dilation angle ($\psi$), flow potential eccentricity ($e$), the ratio of the second stress invariant on the tensile meridian to that on the compressive meridian ($K_c$), a ratio of the compressive strength under biaxial loading to uniaxial compressive strength ($f_{b0}/f_c'$), and a viscosity parameter.

Due to the steel tube's passive confinement, concrete reaches a triaxial stress state when the CFST column is under axial compression [13]. This confinement effect is more significant in circular columns than square columns, as reported in [29].

The concrete elastic material´s behaviour is defined by the modulus of elasticity and Poisson‘s ratio. The plastic part requires the definition of a stress-strain curve for compression and tension in combination with plasticity parameters. The CDP model uses the concept of isotropic damage elasticity in combination with isotropic tensile and compressive plasticity to represent the inelastic behaviour of concrete. Modelling confined concrete behaviour in CFST columns has been challenging and investigated by many authors. The researchers proved that passive confinement would increase both the peak strain (ductility) and the strength of the concrete and the CFST column. One of the possibilities for including the confinement effect in ABAQUS is by modifying the uniaxial concrete stress-strain curve. It means including softening and hardening behaviour as a result of composite action during the lateral expansion of concrete.

### 2.2.2 Concrete models

As mentioned before, this study explores four different stress-strain concrete models. The first three models are the most commonly applied concrete material models in nonlinear 3D FEM analysis of CFST composite columns. The fourth model is the one that follows the concrete material model proposed by EC2 but is extended in order to be applicable for modelling the concrete core inside the steel tube. The corresponding curves for all four models are illustrated in Figure 3 for the geometry and material parameters of specimen 3HN [30], which will be analysed later. Here, $f_c'$ refers to the 150 x 300 mm concrete cylinder compressive strength obtained from tests. A detailed description of all four models follows.

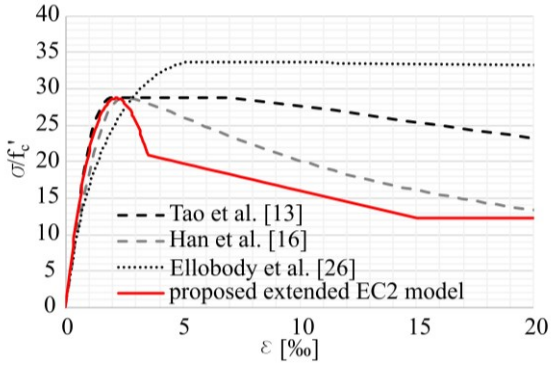


*Figure 3.Concrete constitutive models 1-4 illustrated for material properties of specimen3HN*

#### 2.2.2.1 Concrete material model by Tao et al. [13]

The first evaluated model for concrete is a three-stage $\sigma - \varepsilon$ relation proposed by Tao et al. [13]. This model has been widely exploited as it considers the strain hardening/softening rule of concrete confined by a steel tube. However, it should be noted that this model includes passive confinement since there is an increase in the plastic strain only, and there is no increase in the concrete compressive strength, as presented in Figure 4.

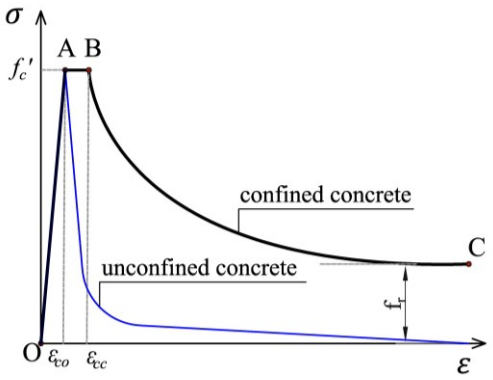


*Figure 4. Stress-strain model for confined concrete used in Model 1*

The first ascending stage between points O-A is defined by equations (2-3) until the peak stress $f_c'$. The peak stress $f_c'$ is the cylinder compressive strength of unconfined concrete. The corresponding strain $\varepsilon_{c0}$ at point A is calculated according to the relationship in equation (4):

$$\frac{\sigma}{f_c'} = \frac{A \cdot X + B \cdot X^2}{1 + (A-2)X + (B+1)X^2} \qquad 0 < \varepsilon \leq \varepsilon_{c0} \tag{2}$$

$$X = \frac{\varepsilon}{\varepsilon_{c0}}, \quad A = \frac{E_c \varepsilon_{c0}}{f_c'} \quad B = \frac{(A-1)^2}{0.55} - 1 \tag{3}$$

$$\varepsilon_{c0} = 0.00076 + \sqrt{(0.626 f_c' - 4.33) \cdot 10^{-7}} \tag{4}$$

$E_c$ is the modulus of elasticity of the unconfined concrete calculated as per ACI 318 [31] with the empirical equation (5) where $f_c'$ is in MPa:

$$E_c = 4700\sqrt{f_c'}[MPa] \quad (5)$$

Further, a second branch is a plateau between points A-B, representing an increased peak strain of concrete due to the confinement. The strain at the point B, $\varepsilon_{cc}$, for the concrete model is determined by the following equation (6):

$$e^k = \frac{\varepsilon_{cc}}{\varepsilon_{c0}}, \quad k = (2.9224 - 0.00367f_c')\left(\frac{f_B}{f_c'}\right)^{0.3124+0.002f_c'} \quad (6)$$

The value $f_B$ represents the confining stress at point B where it is assumed that the ultimate column strength is reached. During the elastic stage, no confining stress is registered as the initial lateral expansion of the concrete is smaller than that of the steel tube. It originates from different values of Poisson's ratio of the composite materials. With the increase in axial strain, the lateral expansion of the concrete core gradually becomes more extensive than the expansion of the steel tube. This mechanism highlights the complexity of the interaction in CFST columns. Here equation (7) is provided for circular CFST columns only, where $D$, $t$, and $f_y$ are the steel tube's outer diameter, wall thickness and yield strength, respectively.

$$f_B = \frac{\left(1 + 0.027f_y\right) \cdot e^{-0.02\frac{D}{t}}}{1 + 1.6 \cdot 10^{-10} \cdot (f_c')^{4.8}} \quad (7)$$

The third stage is the descending branch defined by the following relationship [32]:

$$\sigma = f_r + (f_c' - f_r)exp\left[-\left(\frac{\varepsilon - \boldsymbol{\varepsilon_{cc}}}{\alpha}\right)^{\beta}\right] \ \varepsilon \geq \varepsilon_{cc} \quad (8)$$

in which $f_r$ is the residual stress, while $\alpha$ and $\beta$ are parameters determining the shape of the softening branch. The expressions for $f_r$ and $\alpha$ for circular CFST columns are given in (9) and (10). They are calculated as functions of the so-called "confinement factor" $\xi_c$ (11). It is defined as the ratio between the yield strength $(f_y)$ multiplied by the cross-sectional area of the steel tube $(A_s)$ and the concrete compressive strength $(f_c')$ multiplied by the cross-sectional area of the concrete core $(A_c)$. The parameter $\beta$ in equation (8) has a value of 1.2 for circular CFST columns. Parameters $\alpha, \beta$ and $f_r$ cannot be directly derived from the tests, and their values are proposed based on the regression analysis as the best match for the test curves used in the study [13].

$$f_r = 0.7\left(1 - e^{-1.38\xi_c}\right)f_c' \leq 0.25f_c' \quad (9)$$

$$\alpha = 0.04 - \frac{0.036}{1 + e^{6.86\xi_c - 3.49}} \quad (10)$$

$$\xi_c = \frac{A_s f_y}{A_c f_c'} \quad (11)$$

Concrete tensile behaviour needs to be defined to complete the necessary inputs for the CDP model in ABAQUS. In the current model, the uniaxial tensile response is assumed to be linear until the tensile strength of concrete is reached, which is taken as $0.1f_c'$. Beyond the failure stress, the linear softening response is defined by the fracture energy $G_F$ [33]:

$$G_F = \left(0.469d_{max}^2 - 0.5d_{max} + 26\right)\left(\frac{f_c'}{10}\right)^{0.7} N/mm \quad (12)$$

where $f_c'$ is in MPa, $d_{max}$ is the maximum coarse aggregate size taken as 20mm.

Once the whole material curve is completed, the concrete plasticity parameters must be defined. For the flow potential eccentricity *e* and viscosity parameter, the default values of 0.1 and 0 are adopted. The ratio of the compressive strength under biaxial loading to uniaxial compressive strength $f_{b0}/f_c'$ is calculated by the expression proposed by Papanikolaou and Kappos [34]:

$$f_{b0}/f_c' = 1.52(f_c')^{-0.075} \quad (13)$$

For the remaining CDP parameters, Tao et al. [14] performed the sensitivity analysis and suggested the following expressions:

– dilation angle $\psi$ should depend on the confinement factor $\xi_c$:

$$\psi = \begin{Bmatrix} 56.3(1 - \xi_c)\xi_c \leq 0.5 \\ 6.672e^{\frac{7.4}{4.64 + \xi_c}} \ \xi_c > 0.5 \end{Bmatrix} \quad (14)$$

– the ratio of the second stress invariant on the tensile meridian to that on the compressive meridian $K_c$ should depend on $f_c'$ and be calculated as follow:

$$K_c = \frac{5.5}{5 + 2(f_c')^{0.075}} \quad (15)$$

2.2.2.2 Concrete material model by Han et al.[16]

The second concrete material model discussed here is by Han et al. [16]. It is well known for giving good predictions with the CDP model in ABAQUS [16]. It also relies on the idea that improving the concrete strength under triaxial stress states can be introduced into the FE model through the plastic behaviour of the equivalent stress-strain relationship for concrete. The plasticity of the concrete core confined by a steel tube demonstrates an increase in strain corresponding to the maximum stress and strengthening in the descending branch of the curve. Generally, it defines concrete plastic behaviour depending on the confinement factor $\xi$, equation (16).

$$\xi = \frac{A_s f_y}{A_c f_{ck}} = \alpha \frac{f_y}{f_{ck}} \quad (16)$$

where $A_s$ and $A_c$ are the cross-sectional area of the steel and concrete, respectively; $\alpha(=A_s/A_c)$ is the steel ratio; $f_y$ is the yield strength of the steel; and $f_{ck}$ the characteristic strength of the concrete,which equals $0.67f_{cu}$ for normal strength concrete; $f_{cu}$is the 150 mm cube strength of the concrete.

The following expressions (17-21) define the stress-strain model in Figure 5 proposed for the FE modelling:

$$y = \begin{Bmatrix} 2x - x^2, & (x \leq 1) \\ \frac{x}{\beta_0(x-1)^{\eta} + x}, & (x > 1) \end{Bmatrix}, \quad x = \frac{\varepsilon}{\varepsilon_0} \ , \ y = \frac{\sigma}{\sigma_0} \quad (17)$$

$$\sigma_0 = f_c'\left(\frac{N}{mm^2}\right) \quad (18)$$

$$\varepsilon_c = (1300 + 12f_c')\, x\, 10^{-6} \quad (19)$$

$$\varepsilon_0 = \varepsilon_c + 800\xi^{0.2}\, x\, 10^{-6} \quad (20)$$

where for CFST with circular section:

$$\begin{Bmatrix}\beta_0 = (2.36\,x\,10^{-5})^{[0.25+(\xi-0.5)^7]}(f_c')^{0.5}x\,0.5 \geq 0.12\\ \eta = 2\end{Bmatrix} \quad (21)$$

and $f_c'$ is the compressive cylinder strength of the concrete. The initial modulus of elasticity $E_c$ and Poisson's ratio of 0.2 are taken as recommended in ACI Committee 318 [31], equation (22):

$$E_c = 4730\sqrt{f_c'}[MPa] \quad (22)$$

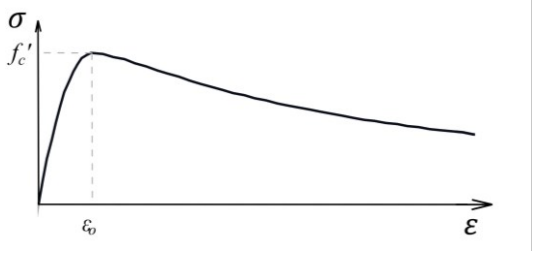


*Figure 5. Stress-strain model for confined concrete used in Model 2*

The model uses the same fracture energy model as in [16] proposed by Hillerborg [35] for concrete in tension.

Finally, Han suggested constant values for the concrete plasticity parameters in the CDP model. Dilation angle ($\psi$), flow potential eccentricity ($e$), the ratio of the second stress invariant on the tensile meridian to that on the compressive meridian ($K_c$), a ratio of the compressive strength under biaxial loading to uniaxial compressive strength ($\frac{f_{b0}}{f_c'}$), and viscosity parameters are taken as 30º, 0.1, 1.16, 2/3 and 0, respectively.

2.2.2.3 Concrete material model by Ellobody [26]

The third considered concrete material model is an idealised uniaxial response for the compressive stress-strain curve for confined concrete proposed by Ellobody. It originates initially from the model proposed by Mander [36] for confined concrete but is adjusted for application in modelling CFST columns. The main inputs to be determined are the confined concrete compressive strength $f_{cc}'$ and corresponding confined strain $\varepsilon_{cc}$ in the equations (23-24) proposed by Mander.

$$f_{cc}' = f_c' + k_1 f_l \quad (23)$$

$$\varepsilon_{cc} = \varepsilon_c\left(1 + k_2\frac{f_l}{f_c'}\right) \quad (24)$$

where $f_c$ is the unconfined concrete cylinder compressive strength. The corresponding unconfined strain $\boldsymbol{\varepsilon_c}$ is taken as 0.003 for plain concrete as the ACI Specification recommends [31]. $f_l$ is the lateral confining pressure imposed by the steel tube and obtained from the empirical equation (25):

$$f_l = \frac{\sigma_\theta t}{D} \quad (25)$$

Where $\boldsymbol{\sigma_\theta}$ is equal to $0.1f_y$ by Mander [36]. The factor $k_1$ is taken as 4.1, and factor $k_2$ 20.5.

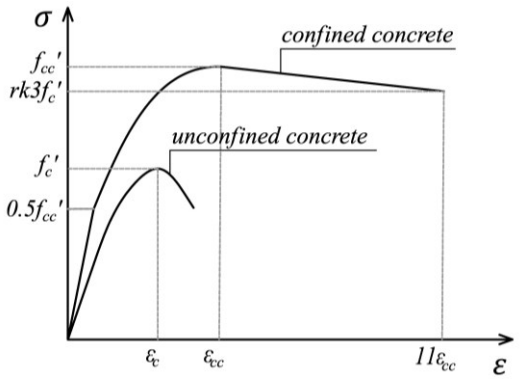


*Figure 6. Stress-strain model for confined concrete used in Model 3*

The uniaxial stress-strain curve consists of three parts, as shown in Figure 6. The first part considers elastic concrete behaviour until the proportional limit stress, which is taken as $0.5f_{cc}$ as per Hu [37].Recommendations also take the initial Young's modulus of confined concrete $E_{cc}$ from the ACI Specification [31]. Poisson's ratio of confined concrete $\nu_{cc}$ is taken as 0.2.

$$E_{cc} = 4700\sqrt{f_{cc}'}[MPa] \quad (26)$$

The second part of the curve between the proportional limit of $0.5f_{cc}$ and confined concrete strength $\boldsymbol{f_{cc}}$ is the nonlinear branch defined by the relation provided in (27).

$$\boldsymbol{\sigma} = \frac{E_{cc}\cdot\varepsilon}{1 + (R + R_E - 2)\cdot\left(\frac{\varepsilon_c}{\varepsilon_{cc}}\right) - (2R-1)\cdot\left(\frac{\varepsilon_c}{\varepsilon_{cc}}\right)^2 + R\cdot\left(\frac{\varepsilon_c}{\varepsilon_{cc}}\right)^3} \quad (27)$$

where $R$ and $R_E$ were computed using the following equations (28-29):

$$R_E = \frac{E_{cc}\cdot\varepsilon_{cc}}{f_{cc}} \quad (28)$$

$$R = \frac{R_E\cdot(R_\sigma - 1)}{(R_\varepsilon - 1)^2} - \frac{1}{R_\varepsilon} \quad (29)$$

In equation (29), $R_\varepsilon$ and $R_\sigma$ are equal to 4,as recommended by [38]. The dilatation angle of 20◦is used in the CDP model, while for the default viscosity parameter, zero value is used. The Poisson coefficient is 0.2 [26].

2.2.2.4 The proposed extended EC2 model

The final considered concrete material model is the EC2 stress-strain relation for the nonlinear structural analysis for short-term uniaxial loading shown in Figure 7. When performing the general nonlinear analysis method for composite columns according to EC4, this is the material model that the engineer is referred to.

The curve in compression is described by the expressions (30-35):

$$\frac{\sigma_c}{f_c'} = \frac{k\eta - \eta^2}{1 + (k-2)\eta} \quad (30)$$

$$k = 1.05\,E_{cm}\cdot\frac{\varepsilon_{c1}}{f_{cm}} \quad (31)$$

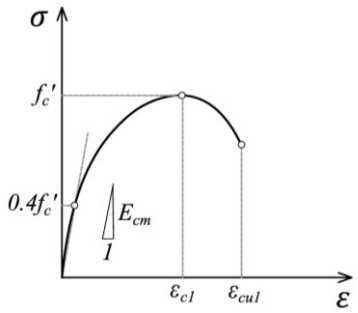


*Figure 7. Schematic representation of the EC2 stress-strain relation for nonlinear structural analysis*

$$E_{cm} = 22 \cdot 10^3 (f_{cm}/10)^{0.33} \quad (32)$$

$$\eta = \frac{\varepsilon_c}{\varepsilon_{c1}} \quad (33)$$

$$\varepsilon_{c1}[‰] = 0.7 f_{cm}{}^{0.31} \leq 2.8\ ‰ \quad (34)$$

$$\varepsilon_{cu1} = 3.5\ ‰, \qquad f_{cm} \leq 58\ MPa \quad (35)$$

where $f_c'$ is the mean cylinder compressive strength, $E_{cm}$ is the secant modulus of elasticity, $\varepsilon_{c1}$ is the strain at peak stress and $\varepsilon_{cu1}$ is the nominal ultimate strain.

However, according to EC2, the stress-strain relation in (30) is only valid for $\varepsilon_c \leq \varepsilon_{cu1} = 3.5\ ‰$, which is insufficient to simulate the increased ductility and the softening behaviour of the CFST column. Therefore, this paper proposes a simple extension of this curve following the recommendations for the numerical modelling of CFST columns provided in [39].

$$\sigma_{res} = \begin{cases} \sigma_{cu1} & \frac{D}{t} \leq 24 \\ \sigma_{cu1}\left(1.6 - 0.025\frac{D}{t}\right) & 24 < \frac{D}{t} \leq 64 \\ 0 & 64 < \frac{D}{t} \end{cases} \quad (36)$$

The residual stress $\sigma_{res}$ calculated from expression (36) depend on the $D/t$ ratio and concrete stress value $\sigma_{cu1}$ at $\varepsilon_{cu1} = 3.5\ ‰$. According to [39], the concrete stress decreases with increasing compressive strain to a residual value ($\sigma_{res}$) at 15‰ strain. Here, it is proposed that the concrete stress $\sigma_c$ decreases linearly beyond the strain limit of 3.5‰ to this residual value $\sigma_{res}$ at 15‰ strain. Further, this stress value remains constant until 20‰ strain, as illustrated in Figure 8.

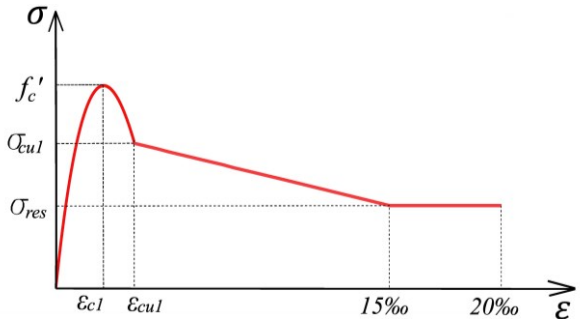


*Figure 8. Proposed stress-strain model for confined concrete used in Model 4*

Model 4 has the same characteristics for concrete in tension as adopted for Model 2. The plasticity parameters are also taken as for Model 2: 30º, 0.1, 1.16, 2/3 and 0, respectively.

### 2.2.3 Material modelling of steel tube

Structural steel properties required for ABAQUS are provided within a uniaxial stress-strain relationship $\sigma - \varepsilon$. Key input parameters for defining the curve are yield strength $f_y$, modulus of elasticity $E$, and the plasticity parameters that depend on the chosen curve. Researchers have investigated different stress-strain constitutive models for carbon steel, such as elastic-perfectly plastic, bilinear, and multilinear with hardening [40], [41].

This paper considered three different constitutive models for steel, schematically illustrated in Figure 9 for specimen 3HN. The first stress-strain curve is proposed by Tao et al. in [13] and consists of an elastic branch until the yield strain $\varepsilon_y$, a perfectly plastic branch until $15\varepsilon_y$ and hardening until the ultimate strain $\varepsilon_u$. Hardening is defined by strain-hardening exponent *p*.

The second is the five-stage elastic-plastic stress-strain model presented by Han et al. in [16]. It consists of elastic, elastic-plastic, plastic, hardening and fracture defined with $\varepsilon_e = 0.8 f_y/E$, $\varepsilon_{e1} = 1.5\varepsilon_e$, $\varepsilon_{e2} = 10\varepsilon_{e1}$, $\varepsilon_{e3} = 100\varepsilon_{e1}$, respectively, where $\varepsilon_e$ is the yield strain and $E$ modulus of elasticity.

The third constitutive model presented is an elastic-perfectly plastic $\sigma - \varepsilon$ relationship for structural steel given in EC3 [27]. Steel material properties used in tests are provided in Table 2. Poisson's ratio is taken as 0.3.

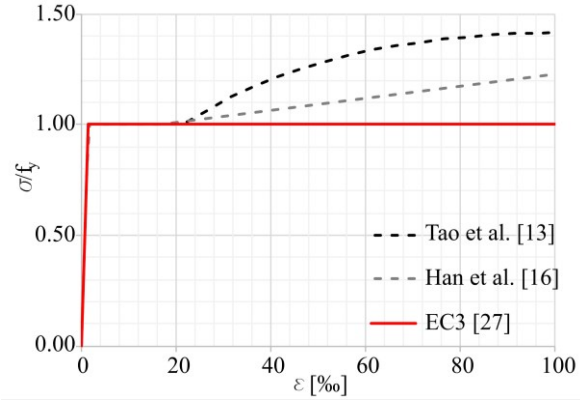


*Figure 9. Steel models used illustrated for material properties of specimen 3HN [30]*

However, this study showed that the choice of the steel stress-strain model does not significantly impact the numerical results. The same observation was previously reported in the literature [5].

## 3 Validation of the proposed 3d models

Proposed models have been validated based on test results provided in the literature. Here the validation is presented on eight short circular specimens with test results from various studies for columns with $L/D \leq 3$ to minimise the member slenderness effects. Table 2 lists the material properties of specimens and their references. The specimens are gradually loaded in all selected experiments with increasing axial loading. The loading is simultaneously applied to the whole cross-section.

*Table 2. Details of specimens with material properties for concrete and steel*

| No. | Specimen and reference | Specimen details | | | | | | Concrete | Steel | | |
|---|---|---|---|---|---|---|---|---|---|---|---|
| | | D | t | L | D/t | L/D | ξ | $f_c'$ | $f_y$ | E | Pois. ratio |
| | | [mm] | [mm] | [mm] | - | - | - | [MPa] | [MPa] | [GPa] | - |
| 1 | 3HN [30] | 150.0 | 3.20 | 450.00 | 46.88 | 3.0 | 1.05 | 28.7 | 7.4 | 200.0 | 0.30 |
| 2 | CC-0 [11] | 139.1 | 2.79 | 420.00 | 49.86 | 3.0 | 0.92 | 41.2 | 388.5 | 203.8 | 0.28 |
| 3 | cfst8-L35-0-a [22] | 140.0 | 2.74 | 420.00 | 51.09 | 3.0 | 0.72 | 40.8 | 309.0 | 181.0 | 0.27 |
| 4 | cfst12-L35-0-b [22] | 140.0 | 3.90 | 420.00 | 35.9 | 3.0 | 1.15 | 40.8 | 335.3 | 205.0 | 0.27 |
| 5 | 310-60-3.6 [24] | 114.0 | 3.60 | 250.00 | 31.67 | 2.2 | 0.83 | 60.0 | 310.0 | 200.0 | 0.30 |
| 6 | 310-60-5.6 [24] | 114.0 | 5.60 | 250.00 | 20.36 | 2.2 | 1.36 | 60.0 | 310.0 | 200.0 | 0.30 |
| 7 | 310-60-3.1 [24] | 167.0 | 3.10 | 250.00 | 53.87 | 1.5 | 0.47 | 60.0 | 310.0 | 200.0 | 0.30 |
| 8 | C1-178-40-C00 [23] | 178.0 | 6.55 | 548.33 | 27.18 | 3.1 | 1.91 | 40.0 | 403.0 | 209.6 | 0.30 |

Figures 10-19 show the axial load–axial strain ($N-\varepsilon$) relations for specimens from Table 2. Diagrams contain results obtained numerically using presented FE Models 1-4 compared to the results obtained from experiments. When results in the test were originally reported as axial load–axial shortening ($N-\Delta$) relations, they are converted by dividing axial shortening $\Delta$ with the column initial length $L$ to obtain ($N-\varepsilon$) relations [9], [13].

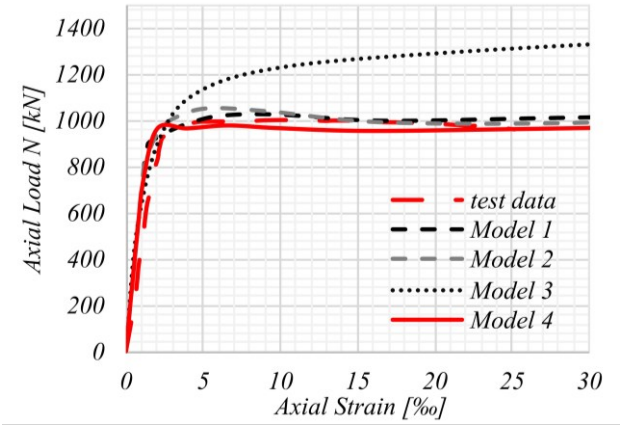


*Figure 10. N-ε diagram for specimen 3HN*

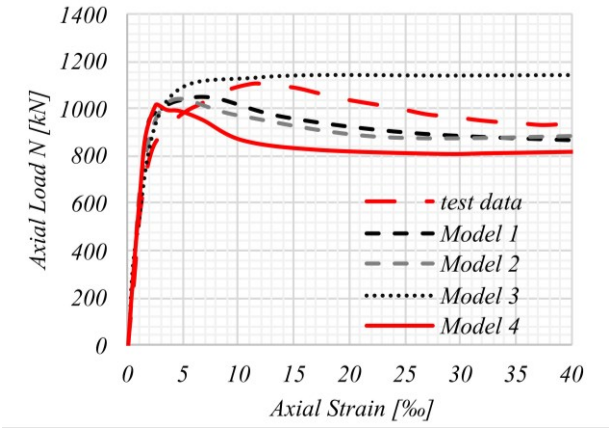


*Figure 12. N-ε diagram for specimen cfst8-L35-0-a*

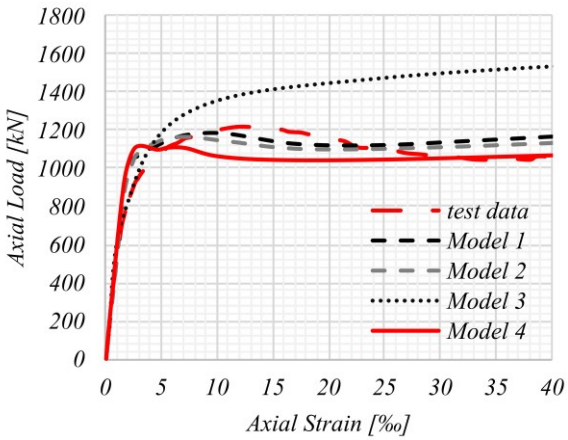


*Figure 11. N-ε diagram for specimen CC-0*

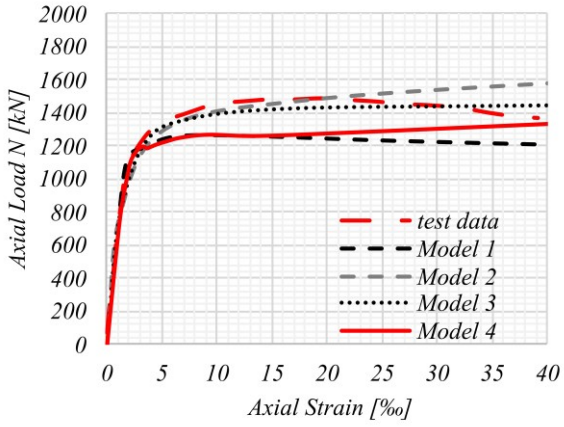


*Figure 13. N-ε diagram for specimen cfst12-L35-0-b*

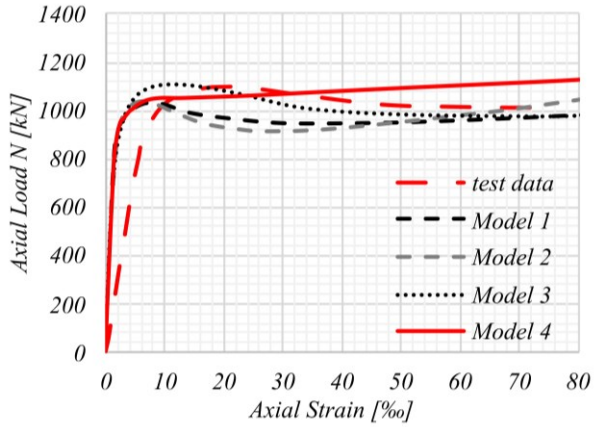


Figure 14. N-ε diagram for specimen 310-60-3.6

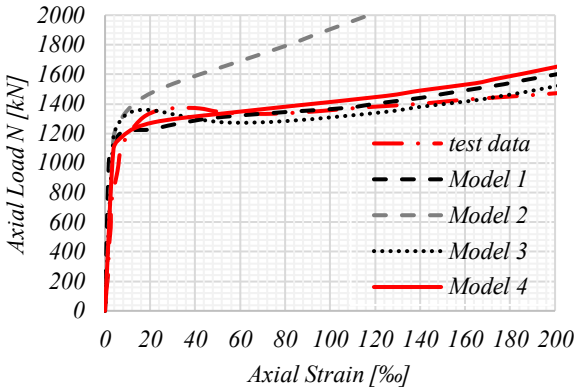


Figure 15. N-ε diagram for specimen 310-60-5.6

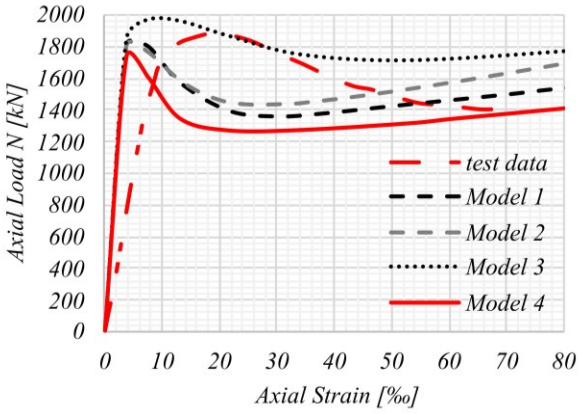


Figure 16. N-ε diagram for specimen 310-60-3.1

Figures 10-17 show that, in general, a satisfactory agreement between the numerical and test results is achieved with all four models regarding the ultimate column capacity. In tests shown in Figures 14, 16, 17, and slightly in Figure 10, the numerical results missed matching the experimental results during the initial elastic stage. This is due to differences in the actual value of the elastic modulus of concrete and the calculated values used in the numerical models. Since the measured values of the elastic modulus of concrete are not reported in all tests, the elastic modulus of concrete is calculated from the corresponding expressions described in Section 2 in all numerical models. Regarding the

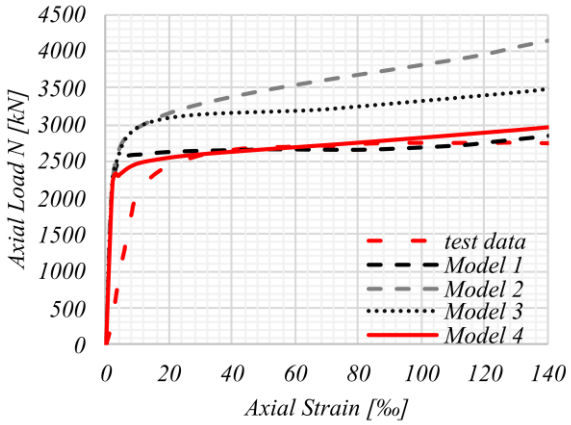


Figure 17. N-ε diagram for specimen C1-178-40-C00

full $N-\varepsilon$ curves, the differences between models are more pronounced. Model 1 has been shown to be the most accurate in this analysis. It successfully simulated CFST column behaviour for most specimens regarding ultimate capacity and the $N-\varepsilon$ response curve. The results obtained by Model 2 have also shown a good correlation with the experimental results for the specimens with a $D/t$ ratio higher than 30. One possible reason for the different behaviour of specimens with a lower $D/t$ ratio is an overestimation of the confinement effect and the strengthening of columns with a ticker steel tube in the post-peak stage. Model 3 gives results that agree well with the experimental results for specimens with concrete strengths higher than 40 MPa. It comes from the Mander concrete material model in Model 3, which considers the increase in concrete ductility and peak strength due to confinement effects. This is not the case for the concrete material models in Models 1 and 2. Finally, the results of Model 4 are in very good agreement with the experimentally obtained results for all tests. These results are similar to those obtained by Model 1. Therefore, the extension of the concrete material model from EC2 enabled Model 4 to capture well the peak and post-peak behaviour of the CFST column.

The shape of the $N-\varepsilon$ response depends on the confinement factor $\xi$ [42][43], equation (16), which varies based on the cross-sectional shape of the column. For different types of CFST's cross-sections, different critical values $\xi_0$ are defined. Circular CFST columns are estimated to be around 1.01 to 1.21 [43]. When the actual confinement factor is less than $\xi_0$ the $N-\varepsilon$ response has a "strain softening" shape. When it is equal to $\xi_0$, the response is "perfectly plastic", while for values of $\xi$ higher than $\xi_0$, the response is of the "strain hardening" type. The value of $\xi$ for each of the analysed specimens is calculated in Table 2. Clearly, this factor is the smallest for specimen 310-60-3.1 (equal to 0.47); therefore, its response exhibits the most noticeable strain-softening shape. The numerical models also predict this softening branch, but due to previously discussed differences in the initial stiffnesses, there are discrepancies between the numerical and experimental responses.

In addition, it should be noted that nonlinear static analysis in ABAQUS using the CDP model is sensitive to the variation of plasticity parameters. Moreover, it should be underlined that the presented specimens belong to different experimental studies. Test data were carefully reviewed to understand the test setup, instrumentation and results, especially in describing the test, steel and concrete material

properties. However, not all necessary data is reported, and the missing values are calculated from the available expressions.

Finally, as mentioned in the introductory part of the paper, one significant advantage of the detailed $3D$ model is its ability to predict the failure modes correctly. All selected specimens experienced very similar drum-like failure modes with or without local buckling of steel tubes near column ends. It should be emphasised that the concrete core within the steel tube postpones or even completely prevents local buckling of the steel tube. All analysed specimens have a $D/t$ ratio well below the limit value according to EC4 (equal to $90 \cdot 235/f_y$) and can be considered not prone to local buckling. Therefore, local buckling effects were not dominant in these tests. Figure 18 shows the numerically obtained failure modes for all analysed specimens. Here, for each test, the figure on the left side (in green) shows the deformed shape in the last calculation step, while the figure on the right side (in colour) shows the vertical displacements (Z direction) for the middle cut of the corresponding specimen. There is a good correlation between the experimental evidence and numerically obtained failure modes.

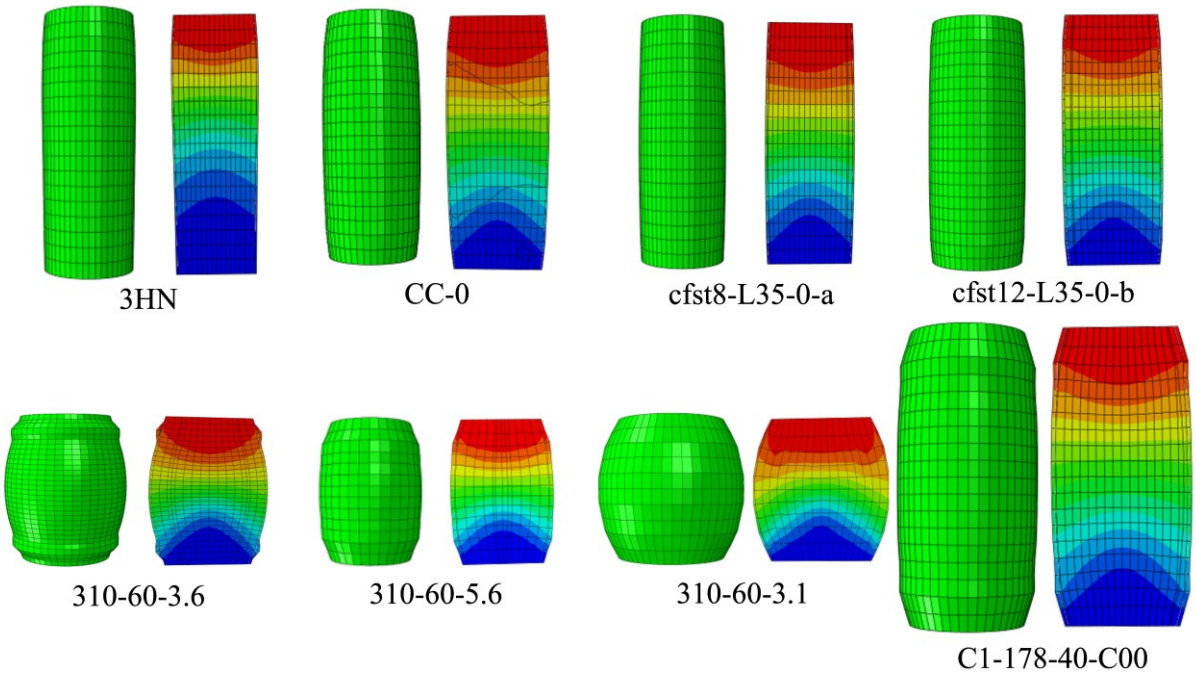


*Figure 18. Deformed shapes of circular stub specimens under axial load*

## 4 Ultimate column compression capacity and comparison with EC4 design code calculations

In this section, the numerically obtained column axial compression capacity $N_{u,i}$from Models $i = 1,2,3,4$ for each specimen is compared with the ultimate strength $N_{u,test}$reported in tests. The value $N_{u,i}$ is determined in the following way. For the specimen with a noticeable peak (maximum) value that is achieved for strains lower than 1%, that value is taken as the ultimate capacity $N_{u,i}$. For specimens that have hardening-type behaviour, the ultimate capacity $N_{u,\mathrm{I}}$ is taken to be equal to the force value corresponding to the strain value of 1%,as suggested by[6]. It should be noted that the test values $N_{u,test}$ are taken to be equal to the values reported by the corresponding authors, although, in some tests, these ultimate strengths correspond to unrealistically high strains (e.g., in test C1-178-40-C00, the ultimate strain is 140 ‰). Also, for each specimen, the ratio $N_{u,i}/N_{u,test}$is calculated, and these values are reported in Table 3. The results show that the average ratios are 93%, 98%, 106% and 91%, respectively, for Models 1 to 4. The corresponding standard deviations are 6%, 5%, 11% and 4%, respectively, for Models 1 to 4. These results lead to similar conclusions as previously derived regarding the whole $N-\varepsilon$ response. Here, Model 2 gives the best predictions with an average ratio of 98% and a standard deviation of 5%. Model 1 and the proposed Model 4 have slightly lower average ratios but still give good predictions of the column's ultimate capacity. The results of Model 3 are the least accurate, with an average ratio of 106% for the $N_{u,i}/N_{u,test}$ and the highest standard deviation.

According to EC4, the resistance to axial compression of a doubly symmetrical and uniform composite cross-section $N_{EC4}$ can be determined using a simplified method of design. The plastic resistance to compression of a composite-cross section should be calculated by adding the plastic resistances of its components, steel tube and concrete core. In the case of concentric loading on concrete-filled tubes of circular cross-sections, $N_{EC4}$ may take into account the decrease in steel strength by a factor $\eta_a$ and the increase in the strength of concrete by a factor $\eta_c$ due to confinement effects, equations (38-39). This confinement effect can be taken into account only if the relative slenderness $\bar{\lambda}$ defined by equation (40) does not exceed 0.5. The effective buckling length of the column $l_0$was taken as $0.5L$, corresponding to the fixed-ended boundary conditions reported in the tests. The values of the $N_{EC4}$ are calculated with material data reported in tests without applying the partial factors for material properties or any other safety factors in the expression (37).

*Table 3. Summary of ultimate axial strength $N_u$ results*

| Specimen | test data | Model 1 | | Model 2 | | Model 3 | | Model 4 | | EC4 | |
|---|---|---|---|---|---|---|---|---|---|---|---|
| | $N_{u,test}$ | $N_{u,1}$ | $\frac{N_{u,1}}{N_{u,test}}$ | $N_{u,2}$ | $\frac{N_{u,2}}{N_{u,test}}$ | $N_{u,3}$ | $\frac{N_{u,3}}{N_{u,test}}$ | $N_{u,4}$ | $\frac{N_{u,4}}{N_{u,test}}$ | $N_{EC4}$ | $\frac{N_{EC4}}{N_{u,test}}$ |
| | [kN] | [kN] | [%] | [kN] | [%] | [kN] | [%] | [kN] | [%] | [kN] | [%] |
| 3HN | 1001 | 1027 | 103% | 1053 | 105% | 1233 | 123% | 980 | 98% | 1175 | 117% |
| CC-0 | 1212 | 1178 | 97% | 1164 | 96% | 1470 | 121% | 1112 | 92% | 1340 | 111% |
| cfst8-L35-0-a | 1143 | 1051 | 92% | 1043 | 91% | 1129 | 99% | 1012 | 89% | 1182 | 103% |
| cfst12-L35-0-b | 1511 | 1260 | 83% | 1408 | 93% | 1400 | 93% | 1269 | 84% | 1476 | 98% |
| 310-60-3.6 | 1095 | 1030 | 94% | 1039 | 95% | 1100 | 100% | 1044 | 95% | 1186 | 108% |
| 310-60-5.6 | 1365 | 1220 | 89% | 1402 | 103% | 1303 | 95% | 1235 | 90% | 1464 | 107% |
| 310-60-3.1 | 1873 | 1805 | 96% | 1804 | 96% | 1967 | 105% | 1738 | 93% | 2091 | 112% |
| C1-178-40-C00 | 2781 | 2579 | 93% | 2905 | 104% | 3050 | 110% | 2465 | 89% | 3134 | 113% |
| *Mean value* | | | *93%* | | *98%* | | *106%* | | *91%* | | *109%* |
| *St dev.* | | | *6%* | | *5%* | | *11%* | | *4%* | | *6%* |

$$N_{EC4} = \eta_a A_s f_y + A_c f_c' \left(1 + \eta_c \frac{t}{D}\frac{f_y}{f_c'}\right) \quad (37)$$

$$\eta_a = 0.25(3 + 2\bar{\lambda}) \leq 1.0 \quad (38)$$

$$\eta_c = 4.9 - 18.5\bar{\lambda} + 17(\bar{\lambda})^2 \geq 0 \quad (39)$$

$$\bar{\lambda} = \sqrt{\frac{N_{pl}}{N_{cr}}} \quad (40)$$

$$N_{pl} = A_a f_y + A_c f_c' \quad (41)$$

$$N_{cr} = \pi^2 \frac{(EI)_{eff}}{{l_0}^2} \quad (42)$$

$$(EI)_{eff} = E_a I_a + 0.6 E_{cm} I_c \quad (43)$$

where:

$N_{pl,Rk}$ is the characteristic value of the plastic resistance to compression,

$N_{cr}$ is the elastic critical normal force for the relevant buckling mode, calculated with the effective flexural stiffness $(EI)_{eff}$,

$I_a, I_c$ are the moments of inertia of the steel section and the concrete section.

The values of $N_{EC4}$ are compared with the experimental data $N_{u,test}$ in the last column of Table 3. The results show that this ratio's mean value and standard deviation are 109% and 6%, respectively. However, the results are not on the safe side, and EC4 overestimates the ultimate strength capacity of the column when calculated with data from the tests. Figure 19 presents a comparison of $N_{u,4}/N_{u,\text{test}}$ ratios obtained for the proposed Model 4 and EC4 predictions. On the other hand, the predictions of the column's ultimate axial capacity obtained by Model 4 are on the safe side for all specimens.

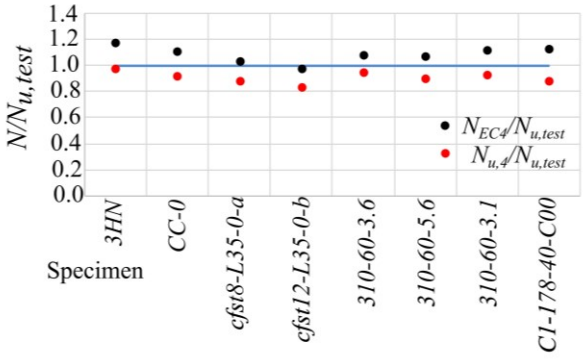


*Figure 19. Model 4-to test and EC4 prediction - to test ultimate strength capacity*

## 5 Conclusion

The paper investigates the numerical modelling of CFST columns' behaviour in ABAQUS software. The presented 3D finite element models simulate the behaviour of circular CFST stub columns under axial compression with high accuracy. The selected four models are validated on a set of experimental tests and have been shown to predict well both: the full $N-\varepsilon$ diagrams and the failure modes. Models 1, 2 and 3 are the most commonly applied models for the nonlinear analysis of CFST columns. Model 1 is proven to simulate the actual behaviour very well for all specimens. Model 2 describes the $N-\varepsilon$ relations very well for specimens with a *D/t* ratio higher than 30 due to overestimating the confinement of the ticker steel tube. Model 3 is the most complex of the selected models regarding consideration of the confinement effects. It provides a good prediction of the full $N-\varepsilon$ column response for specimens with concrete strengths higher than 40 MPa.

The proposed Model 4 is a simple model that shows good agreement with test results regarding the full-range $N-\varepsilon$ diagram. This model overcomes the current limitations of the EC4 and EC2 design guides referring to the limitation of the stress-strain relation by EC2 for concrete in compression to 3.5‰ strain and the absence of a suggested relation for concrete in tension. Also, it considers the concrete core confinement effects. Finally, according to the results of this study, the simplified method of the EC4 for the determination of the short column ultimate compression capacity gives ultimate compression values close to the test values. However, for most of the selected specimens, these values are not on the safe side. The ongoing study investigates this issue in detail on a much larger data set.

### Acknowledgements

The financial support of the Ministry of Education, Science, and Technological Development, Republic of Serbia, through Project 200092, is acknowledged.

### Notation list

| | |
|---|---|
| $D$ | outer diameter of a circular column |
| $L$ | length of a column |
| $t$ | wall thickness of the steel tube |
| $\psi$ | dilation angle |
| $e$ | flow potential eccentricity |
| $K_c$ | ratio of the second stress invariant on the tensile meridian to that on the compressive meridian |
| $f_{b0}/f_c'$ | ratio of the compressive strength under biaxial loading to uniaxial compressive strength |
| $f_c'$ | cylinder compressive strength of unconfined concrete |
| $f_{ck}$ | characteristic strength of the concrete |
| $f_{cu}$ | cube strength of the concrete |
| $f_{cc}'$ | confined concrete compressive strength |
| $f_l$ | lateral confining pressure |
| $\varepsilon_c$ | concrete strain |
| $\varepsilon_{c0}$ | concrete strain at cylinder compressive strength of unconfined concrete |
| $\varepsilon_{cc}$ | concrete strain at peak stress |
| $\varepsilon_y$ | steel yield strain |
| $\varepsilon_u$ | ultimate strain of the steel |
| $E$ | modulus of elasticity of steel tube |
| $E_c$ | modulus of elasticity of the unconfined concrete |
| $E_{cc}$ | modulus of confined concrete |
| $f_B$ | confining stress |
| $f_y$ | yield strength of the steel tube |
| $f_r$ | residual stress |
| $A_s$ | cross-sectional area of the steel tube |
| $A_c$ | cross-sectional area of the concrete core |
| $\xi_c$ | confinement factor |
| $G_F$ | fracture energy |
| $d_{max}$ | maximum coarse aggregate size |
| $\xi$ | confinement factor |
| $E_{cm}$ | secant modulus of elasticity |
| $\varepsilon_{c1}$ | concrete strain at peak stress |
| $\varepsilon_{cu1}$ | concrete nominal ultimate strain |
| $\sigma_c$ | concrete stress |
| $\sigma_{res}$ | concrete residual stress |
| $\Delta$ | column shortening |
| $N_{u,i}$ | column axial compression capacity from Models $i = 1,2,3,4$ |
| $N_{u,test}$ | column test ultimate strength |
| $N_{EC4}$ | resistance to axial compression by EC4 |
| $\eta_a, \eta_c$ | factors related to the confinement of concrete |
| $\bar{\lambda}$ | column relative slenderness |
| $N_{pl,Rk}$ | characteristic value of the plastic resistance to compression |
| $N_{cr}$ | elastic critical normal force for the relevant buckling mode |
| $I_a, I_c$ | moments of inertia of the steel section and the concrete section |

### References

[1] M. M. L. Radovanovic, J. Z. Nikolic, J. R. Radovanovic, and S. M. Kostic, "Structural Behaviour of Axially Loaded Concrete-Filled Steel Tube Columns during the Top-Down Construction Method," *Appl. Sci.*, vol. 12, no. 8, Apr. 2022, doi: 10.3390/app12083771.

[2] S. M. Kostic, F. C. Filippou, and B. Deretic-Stojanovic, "Generalized plasticity model for inelastic RCFT column response," *Comput. Struct.*, vol. 168, pp. 56–67, May 2016, doi: 10.1016/j.compstruc.2016.02.006.

[3] Y. F. Yang and L. H. Han, "Concrete filled steel tube (CFST) columns subjected to concentrically partial compression," *Thin-Walled Struct.*, vol. 50, no. 1, pp. 147–156, Jan. 2012, doi: 10.1016/J.TWS.2011.09.007.

[4] F. xing Ding, W. jun Wang, D. ren Lu, and X. mei Liu, "Study on the behavior of concrete-filled square double-skin steel tubular stub columns under axial loading," *Structures*, vol. 23, pp. 665–676, Feb. 2020, doi: 10.1016/j.istruc.2019.12.008.

[5] Y. Gunawardena and F. Aslani, "Finite element modelling of concrete-filled spiral-welded mild-steel tube short and long columns," *Structures*, vol. 30, pp. 1020–1041, Apr. 2021, doi: 10.1016/j.istruc.2021.01.074.

[6] Z. Bin Wang, Z. Tao, L. H. Han, B. Uy, D. Lam, and W. H. Kang, "Strength, stiffness and ductility of concrete-filled steel columns under axial compression," *Eng. Struct.*, vol. 135, pp. 209–221, Mar. 2017, doi: 10.1016/j.engstruct.2016.12.049.

[7] C. D. Goode, "1819 tests on concrete-filled steel tube columns compared with Eurocode 4," *Struct Eng*, vol. 8, no. 33, p. 86, 2008.

[8] S. Kostic and B. Deretic-Stojanovic, "Fiber element formulation for inelastic frame analysis," *Gradjevinski Mater. i Konstr.*, vol. 59, no. 2, pp. 3–13, 2016, doi: 10.5937/grmk1602003k.

[9] N. Subedi, T. Obara, and S. Kono, “Noncompact and slender concrete-filled steel tubes under axial compression: Finite-element modeling and evaluation of stress-strain models for fiber-based analysis,” *J. Constr. Steel Res.*, vol. 196, Sep. 2022, doi: 10.1016/j.jcsr.2022.107353.

[10] V. I. Patel, Q. Q. Liang, and M. N. S. Hadi, “Nonlinear analysis of axially loaded circular concrete-filled stainless steel tubular short columns,” *J. Constr. Steel Res.*, vol. 101, pp. 9–18, 2014, doi: 10.1016/j.jcsr.2014.04.036.

[11] V. W. Y. Tam, Z. Bin Wang, and Z. Tao, “Behaviour of recycled aggregate concrete filled stainless steel stub columns,” *Mater. Struct. Constr.*, vol. 47, no. 1–2, pp. 293–310, Jan. 2014, doi: 10.1617/s11527-013-0061-1.

[12] Z. Tao, B. Uy, F. Y. Liao, and L. H. Han, “Nonlinear analysis of concrete-filled square stainless steel stub columns under axial compression,” *J. Constr. Steel Res.*, vol. 67, no. 11, pp. 1719–1732, Nov. 2011, doi: 10.1016/j.jcsr.2011.04.012.

[13] Z. Tao, Z. Bin Wang, and Q. Yu, “Finite element modelling of concrete-filled steel stub columns under axial compression,” *J. Constr. Steel Res.*, vol. 89, pp. 121–131, 2013, doi: 10.1016/j.jcsr.2013.07.001.

[14] L. H. Han and Y. F. An, “Performance of concrete-encased CFST stub columns under axial compression,” *J. Constr. Steel Res.*, vol. 93, pp. 62–76, Feb. 2014, doi: 10.1016/j.jcsr.2013.10.019.

[15] M. H. Lai and J. C. M. Ho, “A theoretical axial stress-strain model for circular concrete-filled-steel-tube columns,” *Eng. Struct.*, vol. 125, pp. 124–143, Oct. 2016, doi: 10.1016/j.engstruct.2016.06.048.

[16] L. H. Han, G. H. Yao, and Z. Tao, “Performance of concrete-filled thin-walled steel tubes under pure torsion,” *Thin-Walled Struct.*, vol. 45, no. 1, pp. 24–36, Jan. 2007, doi: 10.1016/j.tws.2007.01.008.

[17] N. F. Hany, E. G. Hantouche, and M. H. Harajli, “Finite element modeling of FRP-confined concrete using modified concrete damaged plasticity,” *Eng. Struct.*, vol. 125, pp. 1–14, Oct. 2016, doi: 10.1016/j.engstruct.2016.06.047.

[18] European committee for standardization, “EN 1994-1-1: Eurocode 4: Design of composite steel and concrete structures-Part 1-1: General rules and rules for buildings,” 2004.

[19] Deretić-Stojanović Biljana, Kostić Svetlana, and Stošić Saša, “Analysis of composite steel and concrete columns,” *Build. Mater. Struct.*, vol. 54, no. 1, pp. 62–79, 2011, [Online]. Available: www.dimk.rs

[20] AIJ, *Recommendations for Design and Construction of Concrete Filled Steel Tubular Structures*. Japan: Architectural Institute of Japan, 2008.

[21] *ABAQUS User Manual 6.9. DS SIMULIA Corp., Providence, Rhode Island, USA, 2009*.

[22] Y. Wang, J. Chen, and Y. Geng, “Testing and analysis of axially loaded normal-strength recycled aggregate concrete filled steel tubular stub columns,” *Eng. Struct.*, vol. 86, pp. 192–212, Mar. 2015, doi: 10.1016/j.engstruct.2015.01.007.

[23] V. da S. de Azevedo, L. R. O. de Lima, P. C. G. d. S. Vellasco, M. E. d. N. Tavares, and T. M. Chan, “Experimental investigation on recycled aggregate concrete filled steel tubular stub columns under axial compression,” *J. Constr. Steel Res.*, vol. 187, Dec. 2021, doi: 10.1016/j.jcsr.2021.106930.

[24] F. Abed, M. Alhamaydeh, and S. Abdalla, “Experimental and numerical investigations of the compressive behavior of concrete filled steel tubes (CFSTs),” *J. Constr. Steel Res.*, vol. 80, pp. 429–439, Jan. 2013, doi: 10.1016/j.jcsr.2012.10.005.

[25] D. Lam, X. H. Dai, L. H. Han, Q. X. Ren, and W. Li, “Behaviour of inclined, tapered and STS square CFST stub columns subjected to axial load,” *Thin-Walled Struct.*, vol. 54, pp. 94–105, May 2012, doi: 10.1016/J.TWS.2012.02.010.

[26] E. Ellobody, “Numerical modelling of fibre reinforced concrete-filled stainless steel tubular columns,” *Thin-Walled Struct.*, vol. 63, pp. 1–12, 2013, doi: 10.1016/j.tws.2012.10.005.

[27] European committee for standardization, “EN 1993-1-1: Eurocode 3: Design of steel structures - Part 1-1: General rules and rules for buildings,” 2005.

[28] European committee for standardization, “EN 1992-1-1: Eurocode 2: Design of concrete structures - Part 1-1: General rules and rules for buildings,” 2004.

[29] G. B. Hajjar JF, “A cyclic nonlinear model for concrete-filled tubes formulation.,” *J Struct Eng, ASCE*, no. 123(6), pp. 736–44, 1997.

[30] Y. M. M. Tomii, K. Yoshimura, “Experimental studies on concrete filled steel tubular stub columns under concentric loading,” in *Proceedings of the International Colloquium on Stability of Structures under Static and Dynamic Loads*, 1977, pp. 718–741.

[31] American Concrete Institute, *Building Code Requirements for Structural Concrete (ACI 318-11) and Commentary*. MI, USA: Farmington Hills, 2011.

[32] B. Binici, “An analytical model for stress–strain behavior of confined concrete,” *Eng. Struct.*, vol. 27, no. 7, pp. 1040–1051, Jun. 2005, doi: 10.1016/J.ENGSTRUCT.2005.03.002.

[33] Z. P. Bažant and E. Becq-Giraudon, “Statistical prediction of fracture parameters of concrete and implications for choice of testing standard,” *Cem. Concr. Res.*, vol. 32, no. 4, pp. 529–556, Apr. 2002, doi: 10.1016/S0008-8846(01)00723-2.

[34] V. K. Papanikolaou and A. J. Kappos, “Confinement-sensitive plasticity constitutive model for concrete in triaxial compression,” *Int. J. Solids Struct.*, vol. 44, no. 21, pp. 7021–7048, Oct. 2007, doi: 10.1016/J.IJSOLSTR.2007.03.022.

[35] A. Hillerborg, M. Modéer, and P.-E. Petersson, “Analysis of crack formation and crack growth in concrete by means of fracture mechanics and finite elements,” *Cem. Concr. Res.*, vol. 6, no. 6, pp. 773–781, Nov. 1976, doi: 10.1016/0008-8846(76)90007-7.

[36] J. B. . M. J. P. and R. P. Mander, “Theoretical stress-strain model for confined concrete,” *J. Struct. Eng.*, vol. 114, no. 8, pp. 1804–1826, 1988.

[37] H.-T. Hu, C.-S. Huang, M.-H. Wu, and Y.-M. Wu, “Nonlinear Analysis of Axially Loaded Concrete-Filled Tube Columns with Confinement Effect,” *J. Struct. Eng.*, vol. 129, no. 10, pp. 1322–1329, Oct. 2003, doi: 10.1061/(ASCE)0733-9445(2003)129:10(1322).

[38] H. Hu and W. C. Schnobrich, “Constitutive Modeling of Concrete by Using Nonassociated Plasticity,” *J. Mater. Civ. Eng.*, vol. 1, no. 4, pp. 199–216, 1989, doi: 10.1061/(asce)0899-1561(1989)1:4(199).

[39] J. M. Portolés, M. L. Romero, F. C. Filippou, and J. L. Bonet, “Simulation and design recommendations of eccentrically loaded slender concrete-filled tubular columns,” *Eng. Struct.*, vol. 33, no. 5, pp. 1576–1593, May 2011, doi: 10.1016/j.engstruct.2011.01.028.

[40] E. Ellobody, "Nonlinear behaviour of eccentrically loaded FR concrete-filled stainless steel tubular columns," *J. Constr. Steel Res.*, vol. 90, pp. 1–12, 2013, doi: 10.1016/j.jcsr.2013.07.018.

[41] M. M.A. Kadhim, "Numerical modelling of concrete-filled stainless steel slender columns loaded eccentrically," *World J. Eng.*, vol. 17, no. 5, pp. 697–707, Aug. 2020, doi: 10.1108/WJE-09-2019-0268.

[42] L. H. . Z. X. L. . & T. Z. Han, "Tests and mechanics model for concrete-filled SHS stub columns, columns and beam-columns," *Steel Compos. Struct.*, vol. 1, no. 1, pp. 51–74, 2001.

[43] W. Q. Lyu, L. H. Han, and C. Hou, "Axial compressive behaviour and design calculations on recycled aggregate concrete-filled steel tubular (RAC-FST) stub columns," *Eng. Struct.*, vol. 241, Aug. 2021, doi: 10.1016/j.engstruct.2021.112452.